Electronic Supplementary Material (ESI) for Journal of Materials Chemistry C.
This journal is © The Royal Society of Chemistry

Electronic Supplementary Information

A molecular acceptor with absorption wavelength of >1400 nm for short-wavelength infrared organic photodetectors

Tingting Yuan,[ab] Wenliang Chen,[ab] Junhui Miao*[a] and Jun Liu*[ab]

[a]State Key Laboratory of Polymer Physics and Chemistry, Changchun Institute of Applied Chemistry, Chinese Academy of Sciences, Changchun, 130022, China.

[b]University of Science and Technology of China, Hefei, 230026, China.

E-mail: jhmiao@ciac.ac.cn; liujun@ciac.ac.cn.

Contents

12. Photocurrent *J-V* graph of the OPD device

13. The stability of the material and the OPD device

14. The summary table of ultra-narrow band gap acceptor materials for OPD

15. ^{1}H NMR , ^{13}C NMR and mass spectra

1. Experimental details

General. ^{1}H NMR and ^{13}C NMR spectra were measured with a Bruker AV-400 MHz NMR spectrometer at room temperature. Elemental analysis was recorded on a VarioEL elemental analyzer. 2D grazing incidence wide angle X-ray scattering (2D-GIWAXS) were measured at the BL02U2 beamline at Shanghai Synchrotron Radiation Facility. Samples of pure materials or blends were prepared on silicon substrates. UV-vis absorption spectra (in CF solution and as thin films) were obtained with a Shimadzu UV-3600 spectrometer. Cyclic voltammogram (CV) measurements were performed on a CHI660a electrochemical workstation using glassy carbon as the working electrode, Pt wire as the counter electrode, and a standard calomel reference electrode in a 0.1 mol L^{-1} tetrabutylammonium hexafluorophosphate (Bu_4NPF_6) acetonitrile solution. The materials were casted on the working electrode for measurements and ferrocene as an internal reference at a scan rate of 100 mV s^{-1}. The highest occupied molecular orbital (HOMO) and the lowest unoccupied molecular orbital (LUMO) energy levels of the materials were estimated by the equations: $E_{\mathrm{HOMO/LUMO}} = -(4.80 + \mathrm{E}_{\mathrm{onset}}^{\mathrm{ox}}/\mathrm{E}_{\mathrm{onset}}^{\mathrm{red}})$ eV. The AFM images were recorded using a SPA300HV (Seiko Instruments, Inc., Japan) in tapping mode. The thermogravimetric analysis (TGA) was performed on a Perkin-Elmer 7 instrument at a heating rate of 10 °C min^{-1} under purified nitrogen gas (N_2) flow. The decomposition temperature (T_{d}) corresponded to 5% loss of weight.

2. Syntheses and characterizations

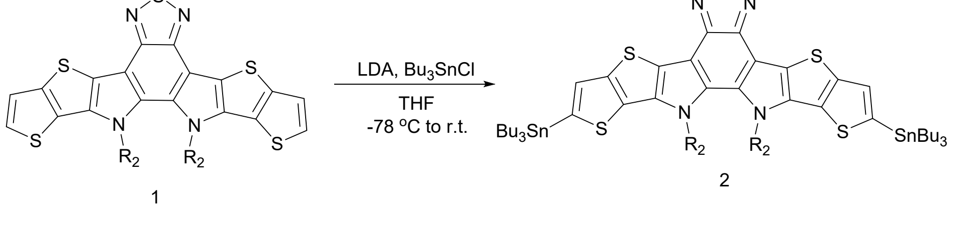

Compound 2: To a solution of compound **1** (0.6 g, 0.77 mmol) in anhydrous tetrahydrofuran (70 mL) at −78 °C was added dropwise LDA (2 M in hexane, 0.82 mL, 1.63 mmol). After the mixture being stirred at –78 °C for 3 h, Bu_3SnCl (2.0 g, 10.1 mmol) was added under argon. The mixture was stirred overnight from –78 °C to 25

°C. After adding KF aqueous solution, the mixture was extracted using ether. The solution was dried using Na_2SO_4, and then concentrated under reduced pressure to afford compound **2** (1.0 g) as a yellow oil. Without any further purification, the product was used into the following reaction.

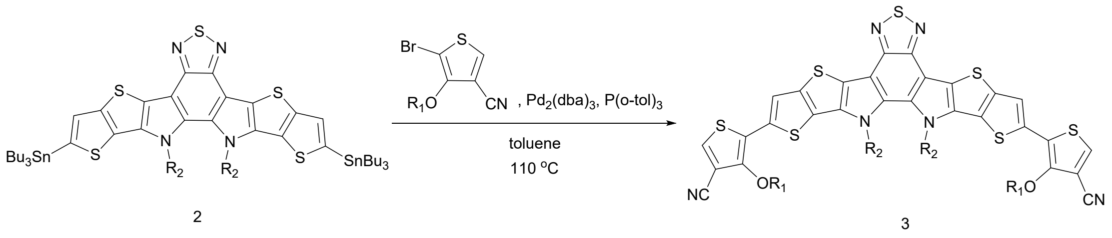

Compound 3: Starting materials of compound **2** (1.0 g, 0.74 mmol), 5-bromo-4-((2-ethylhexyl)oxy)thiophene-3-carbonitrile (0.54 g, 1.7 mmol), $Pd_2(dba)_3$ (67.7 mg, 0.07 mmol) and $P(o\text{-}tol)_3$ (89.96 mg, 0.29 mmol) were placed in a two-necked flask under argon, and then dried toluene (66 mL) was added. After the mixture being stirred at 110 °C for 12 h. The reaction mixture was poured into water, then extracted with dichloromethane three times. The combined organic phase was washed with brine, dried over anhydrous Na_2SO_4, filtered, and concentrated in vacuum. Finally, the residue was purified by silica gel chromatography (petroleum ether/dichloromethane = 1:1, v/v) to afford compound **3** (0.46 g, yield: 47.17%) as a orange oily liquid. ^1H NMR (500 MHz, $CDCl_3$) δ 7.72 (s, 2H), 7.59 (s, 2H), 4.61 (d, J=5 Hz, 4H), 4.27 (d, J=5 Hz, 4H), 2.08 (m, 2H), 1.91 (m, 2H), 1.57 – 1.69 (m, 12H), 1.46 – 1.54 (m, 4H), 1.41 – 1.46 (m, 20H), 1.01 (t, J = 7.5 Hz, 12H), 0.92 (t, J = 8.5 Hz, 12H), 0.61 – 0.67 (m, 12H).

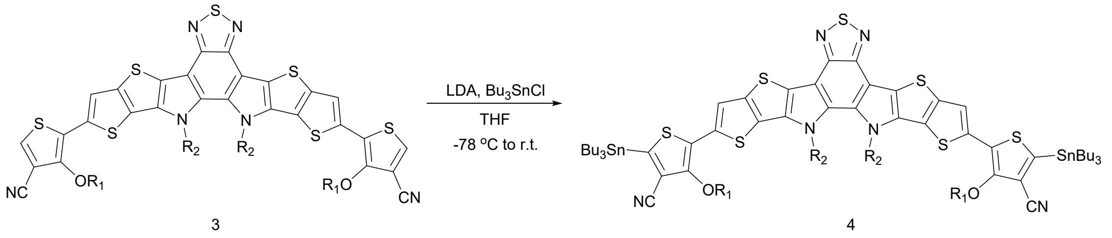

Compound 4: To a solution of compound **4** (0.46 g, 0.35 mmol) in anhydrous tetrahydrofuran (25 mL) at −78 °C was added dropwise LDA (2 M in hexane, 0.37 mL, 0.73 mmol). After the mixture being stirred at –78 °C for 3 h, Bu_3SnCl (0.26 g, 0.80

mmol) was added under argon. The mixture was stirred overnight from –78 °C to 25 °C. After adding KF aqueous solution, the mixture was extracted using ether. The solution was dried using Na_2SO_4, and then concentrated under reduced pressure to afford compound **4** (0.67 g) as a yellow oil. Without any further purification, the product was used into the following reaction.

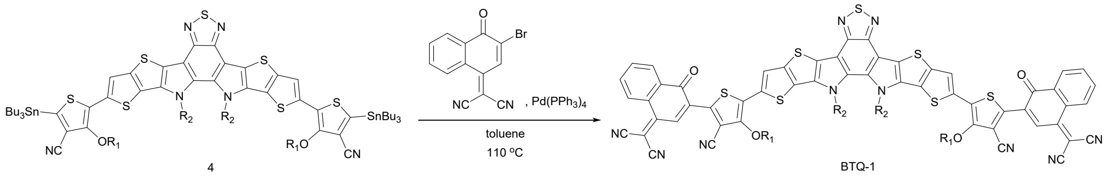

BTQ-1: Starting materials of compound **4** (0.67 g, 0.35 mmol), 2-(3-bromo-4-oxonaphthalen-1(4*H*)-ylidene)malononitrile (0.22 g, 0.77 mmol) and $Pd(PPh_3)_4$ (40.4 mg, 0.03 mmol) were placed in a two-necked flask under argon, and then dried toluene (20 mL) was added. After the mixture being stirred at 110 °C for 12 h. The reaction mixture was poured into water, then extracted with dichloromethane three times. The combined organic phase was washed with brine, dried over anhydrous Na_2SO_4, filtered, and concentrated in vacuum. Finally, the residue was purified by silica gel chromatography (petroleum ether/dichloromethane = 1:1, v/v) to afford BTQ-1 (0.31 g, yield: 52.31%) as a orange oily liquid. ^{1}H NMR (500 MHz, $CDCl_3$) δ 8.85 (d, J=10 Hz, 4H), 8.36 (d, J=5 Hz, 2H), 7.83 – 7.88 (m, 4H), 7.79 (s, 2H), 4.65 (m, 4H), 4.35 (d, J=10 Hz, 4H), 2.15 (m, 2H), 2.01 (m, 2H), 1.51 – 1.76 (m, 12H), 1.35 – 1.48 (m, 12H), 0.92 – 1.08 (m, 36H), 0.64 – 0.70 (m, 12H). ^{13}C NMR (126 MHz, $CDCl_3$) δ 118.82, 154.68, 152.00, 147.49, 142.28, 137.00, 134.54, 134.35, 134.05, 132.67, 131.24, 130.36, 129.91, 129.41, 129.07, 128.26, 126.43, 125.59, 125.31，150.05, 114.44, 114.19, 112.95, 112.41, 105.85, 84.62, 78.39，55.35, 40.61, 38.77, 31.58, 30.21, 29.14, 27.98, 25.36, 23.61, 23.17, 22.80, 22.50, 14.20, 14.00, 13.78, 11.23. MS (MALDI-TOF): Calculated for $C_{94}H_{96}N_{10}O_4S_7$ [M^+], 1652.6; found, 1652.6.

3. Thermal properties

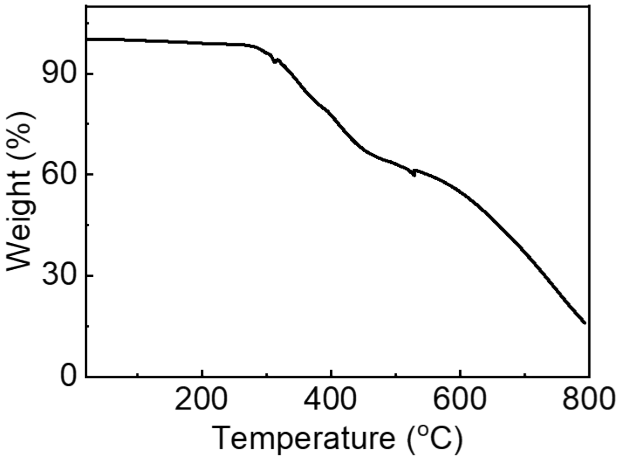

Figure S1. TGA curve of BTQ-1 under N_2 atmosphere at a scan rate of 10 °C min^{-1}. The T_d of BTQ-1 are 308 °C, respectively.

Table S1. Thermal properties and opto-electronic properties of BTQ-1.

Compound	T_d (°C)	λ_{max}^{sol} (nm)	λ_{max}^{film} (nm)	$E_g^{opt\ a)}$ (eV)	$E_{LUMO}^{\ b)}$ (eV)	$E_{HOMO}^{\ b)}$ (eV)	$\mu_e^{\ c)}$ (cm^2 V^{-1} s^{-1})
BTQ-1	308	899	1009	0.79	−4.35	−5.29	2.85×10^{-4}

[a)] Calculated with the onset absorption wavelength in film;

[b)] Calculated from onset oxidation/reduction potentials in CV;

[c)] Measured by the SCLC method.

4. Density functional theory (DFT) calculations

The molecular geometry and wave function distribution of frontier molecular orbitals were calculated using the B3LYP method with 6-31G(d) basis set. To simplify the calculation, the branched alkyl chains were replaced with methyl groups. All visualizations obtained from computed results were generated by the GaussianView 6 program.

5. nuclear independent chemical shift (NICS) values of the aromatic rings of BTQ-1 and BTQ-1-NQC

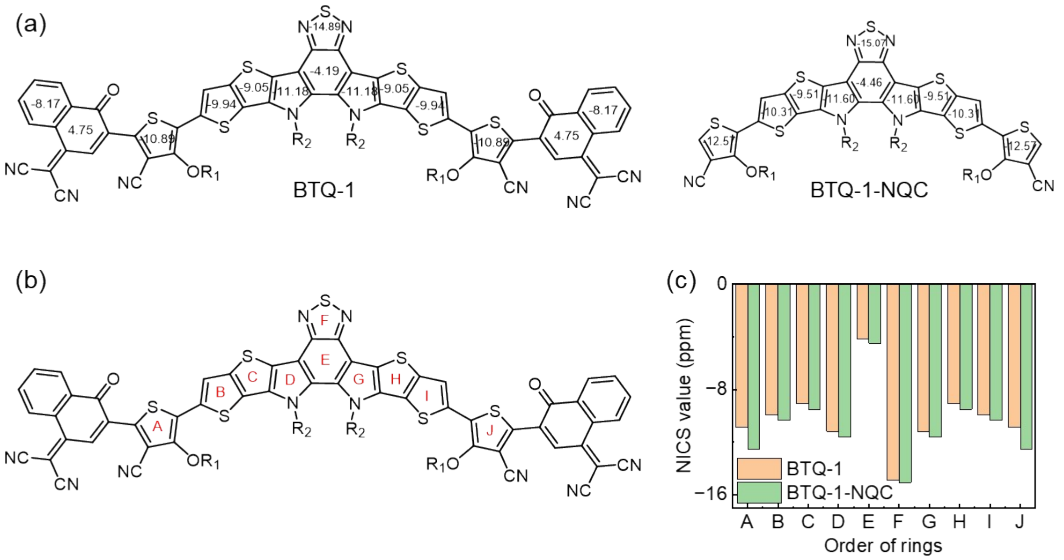

Figure S2. Nucleus-independent chemical shifts

6. Morphology of the blend film

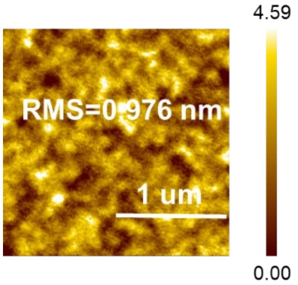

Figure S3. AFM height image of the BHJ film.

The PTB7-Th:BTQ-1 blend film exhibited a uniform surface with a low root-mean-square (RMS) roughness of 0.976 nm.

7. Absorption data of the PTB7-Th:BTQ-1 blend film

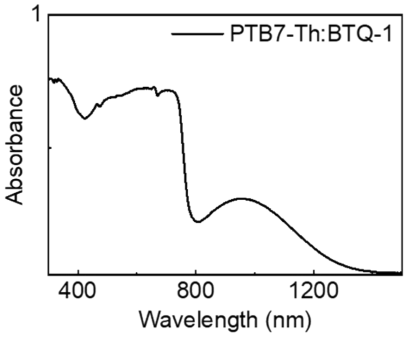

Figure S4. Absorption data of the PTB7-Th:BTQ-1 blend film.

8. 2D-GIWAXS pattern and the corresponding in-plane and out-of-plane linecuts of PTB7-Th

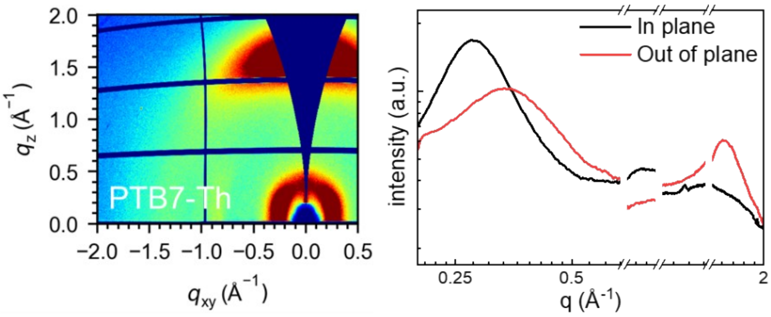

Figure S5. 2D-GIWAXS pattern and the corresponding in-plane and out-of-plane linecuts of PTB7-Th

Table S2. GIWAXS characterization data of the BTQ-1, PTB7-Th and PTB7-Th:BTQ-1 films.

		(100)				(010)			
Film	Direction	Location [Å^{-1}]	d-spacing [Å]	FWHM [Å^{-1}]	CCL [Å]	Location [Å^{-1}]	d-spacing [Å]	FWHM [Å^{-1}]	CCL [Å]
BTQ-1	In-plane	0.36	17.45	0.137	41.3				
	Out-of-plane					1.70	3.70	0.262	21.6
PTB7-Th	In-plane	0.29	21.67	0.066	85.7				
	Out-of-plane	0.39	16.11	0.141	40.1	1.57	4.00	0.170	33.3
PTB7-Th:BTQ-1	In-plane	0.29	21.67	0.092	61.5				
	Out-of-plane	0.32	19.63	0.091	62.1	1.69	3.72	0.248	22.8

9. OPD devices fabrication and measurement

The OPD devices were fabricated with the structure of ITO/ZnO/active layer/MoO$_3$/Al. ITO glass substrates were cleaned in an ultrasonic bath with deionized water, acetone, and isopropyl alcohol, and then dried at 125 ^{o}C for 30 min. After being treated with ultraviolet–ozone for 15 min, ZnO layers (ca. 30 nm) were spin-coated at 5000 r min^{-1} onto the cleaned ITO glasses from the ZnO precursor solution, and then baked at 200 ^{o}C for 60 min in air. The ZnO precursor was synthesized by dissolving zinc acetate dehydrate (200 mg) and ethanolamine (65 mg) in 2 mL 2-methoxyethanol under vigorous stirring for 10 h in air. All of the substrates were placed into a nitrogen-filled glove box. Subsequently, PTB7-Th:BTQ-1 (1:1.2 weight ratio) based blends were dissolved in CF with a concentration of 15.0 mg/mL. The solutions were stirred at 55 ^{o}C for 4 h and then spin-coated onto the substrates at room temperature to obtain the active layers. And then, the active layers were thermal annealed at 110 ^{o}C for 10 min. After that, the device fabrication was completed by thermally evaporating MoO_3 (15 nm) and Al (100 nm) under vacuum at a pressure of 2×10^{-4} Pa. The active area of each device was 8 mm^2.

The current density (J-V) curve of the OPDs was measured by the computer-controlled Keithley 2400 source meter. Simulated solar light illumination was provided by XES-40S2-CE class solar simulator (Japan, SAN-EI Electric Co., Ltd). The EQE data was collected using the CEL-PD291 photodetection performance test system. The LFN-2000 was used to analyze the noise current, the CEL-PD291 light detection performance test system and the RIGOL DS1102 digital oscilloscope were used to analyze the frequency response characteristics.

10. OPD device performance

Table S3. OPD characteristics

Device	R (mA W^{-1})	EQE (%)	S_n (A Hz$^{-1/2}$)	D^* (Jones)	J_d (A cm^{-2})	LDR (dB)	τ_r/τ_f (μs)
PTB7-Th:BTQ-1	3.60/940 nm 0.46/1310 nm	0.48/940 nm 0.04/1310 nm	3.0×10^{-13}	3.42×10^{9}/940 nm 4.3×10^{8}/1310 nm	3.04×10^{-8}	97	93/58

11. Hole/electron-only devices fabrication and hole/electron mobility measurement

Hole-Only and Electron-Only Devices: The hole-only device structure is ITO/PEDOT:PSS/PTB7-Th:BTQ-1/MoO_3/Al and the electron-only device structure is ITO/ZnO/PTB7-Th:BTQ-1/PFN-Br/Al.

The current-voltage curves in the range of 0-8 V were recorded using a computer-controlled Keithley 2400 source meter, and the results were fitted to a space-charge limited function:

$$J = \frac{9}{8}\varepsilon_r \varepsilon_0 \mu \frac{V^2}{L^3} \exp\left(0.89\beta \frac{\sqrt{V}}{\sqrt{L}}\right)$$

where J is the current density, ε_0 is the permittivity of free space, ε_r is the relative permittivity of 3 for molecules, μ is the zero-field mobility, V is the potential across the device ($V = V_{\text{applied}} - V_{\text{bias}} - V_{\text{series}}$), L is the thickness of active layer, and β is the field-activation factor. The series and contact resistance (V_{series}) of the device (10–15 Ω) were measured using blank device of ITO/ZnO/MoO_3/Al. The range of 0-4 V was used to extract the mobility values.

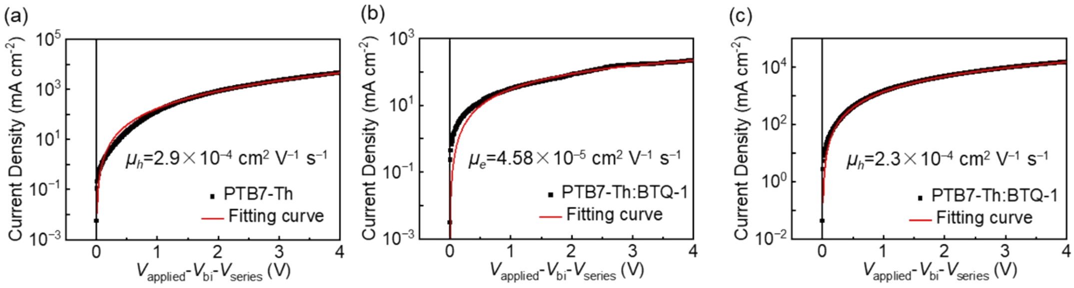

Figure S6. *J–V* curves and SCLC fittings the (a) hole-only devices based on PTB7-Th film; (b) the electron-only devices and (c) the hole-only devices based on PTB7-Th:BTQ-1 blend.

12. Photocurrent *J-V* graph of the OPD device

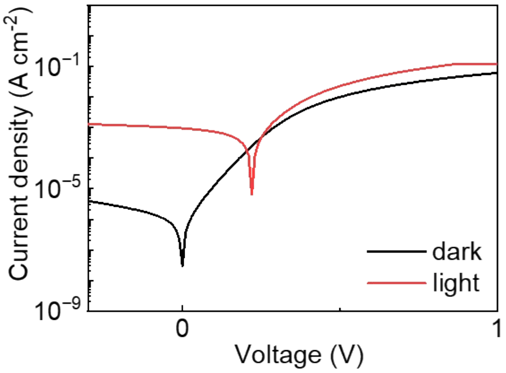

Figure S7. Photocurrent J-V graph of the OPD device.

13. The stability of materials and OPD devices

The intensity of the maximum absorption peak in the infrared region of the BTQ-1 film, both in air and under heating conditions, did not change significantly, indicating that the film exhibits relatively good air stability and thermal stability.

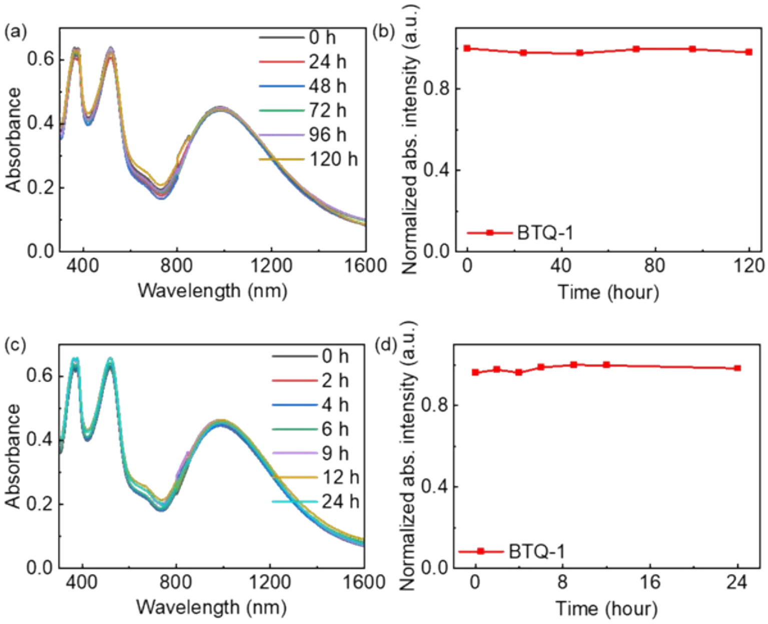

Figure S8. (a) Absorption spectra of BTQ-1 stored in air for different times and (b) the decay curve of the maximum absorption peak in the infrared region; (c) Absorption spectra of BTQ-1 heated at 110 °C for different times and the (d) decay curve of the maximum absorption peak in the infrared region.

We tested the air stability of the OPD device based on PTB7-Th:BTQ-1. Figure S9 shows the change curve of the dark current and normalized photocurrent stored in air for 0 min~600 min. The dark current exhibited relatively high stability and remained largely unchanged. However, the photocurrent decreased to 80 % of the initial value at 240 min. This decrease in photocurrent may be due to changes in the phase-separated morphology of the optimized active layer upon exposure to air, which in turn affects carrier transport and deteriorates device performance.

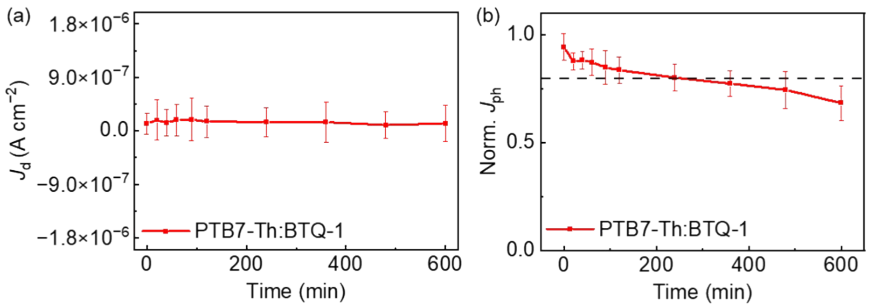

Figure S9. Stability of the J_d and normalized J_{sc} of OPD after storage in air atmosphere for different times.

14. The summary table of ultra-narrow band gap acceptor materials for OPD

Table S4. Ultra-narrow band gap acceptor materials for OPD

Active layers	E_g^{opt} (eV)	Bias (V)	J_d (A cm^{-2})	R (A W^{-1})	D^* (Jones)	Reference
PBDB-T/DO-4F(thick)	1.24	0	8.6×10^{-10}	0.50/850 nm	3.05×10^{13} [b]	[1]
D18/FM-8F	1.24	−5	5.2×10^{-7}	0.46/970 nm	1.44×10^{12}	[2]
PTB7-Th/YOR1	1.24	−0.1	1.58×10^{-10}	0.14/950 nm	1.29×10^{12}	[3]
PBDB-T/FM2	1.22	−0.5	6.45×10^{-9}	0.45/880 nm	1.01×10^{13}	[4]
PM6/PDTTYM	1.22	0	3.9×10^{-9}	0.48/900 nm	1.31×10^{13} [b]	[5]
P3HT/TPBT-OR	1.20	−0.1	3.57×10^{-8}	0.084/850 nm	6.32×10^{11}	[6]
PM6/PDTTIC-4F(thick)	1.20	0	1.64×10^{-9}	0.48/920 nm	2.40×10^{13} [b]	[7]
PM6/O4TFIC	1.20	0	8.3×10^{-5} [c]	0.50/890 nm	9.0×10^{11}	[8]
PTB7-Th:CO1-4F	1.20	−3	8.0×10^{-5}	0.52/920 nm	2.6×10^{10}	[9]
PBDB-T/BPPT-4Cl	1.19	0	2.1×10^{-15} [a]	0.34/870 nm	2.2×10^{13}	[10]
PTB7-Th/CO1-4Cl	1.19	−2	7×10^{-9}	0.5/960 nm	3.13×10^{13} [b]	[11]
PTB7-Th:BFIC	1.18	0	4.4×10^{-11}	>0.3/710~950 nm	5.46×10^{13}	[12]
PCE10/YZ1	1.18	0	5.3×10^{-11}	0.27/1000 nm	1.4×10^{13}	[13]
PCE10/BTPV-4F-eC9	1.18	0	4.65×10^{-10}	0.56/900 nm	1.14×10^{13} [b] /1030 nm	[14]
PTB7-Th/tSPT-4F	1.17	−0.1	4.52×10^{-10}	0.40/1010 nm	1.25×10^{13}	[15]
PTB7-Th/CBT	1.14	−0.5	5.22×10^{-8}	0.455/880 nm	3.29×10^{12}	[16]
PTB7-Th/COTH	1.13	−0.5	3.34×10^{-6}	0.26/1000 nm	2.74×10^{11} [b]	[17]
PTB7-Th/COT-Oct	1.13	−0.5	8.18 × 10−9	0.24/1000 nm	1.49×10^{12} [b]	[18]
PTB7-Th/NTQ	1..11	−0.1	1.5×10^{-7}	0.24/970 nm	3.72×10^{12} [b] /1000 nm	[19]
PBDT-TT/DPPSe-4Cl/Y6	1.11	−0.1	1.0×10^{-9}	0.18/940 nm	1.0×10^{13} [b]	[20]
PTB7-Th/COTIC-4F	1.10	0	1.4×10^{-8}	0.37/995 nm	1.7×10^{11} [b]	[9]

PBDB−T/OTB4	1.09	0	6.40×10^{-10}	0.036/1180 nm	2.98×10^{11}	[21]
PTB7-Th/COB	1.08	−0.5	5.22×10^{-8}	0.37/1050 nm	2.68×10^{12}	[16]
PCE10/TPA-4F	1.08	−0.1	2.61×10^{-10}	0.25/1100 nm	2.67×10^{13}	[22]
PCE10/FB-C6	1.07	−0.1	4.59×10^{-8}	0.29/970 nm	4.94×10^{11}	[23]
PTB7-Th/COTCN2	1.05	−0.5	1.08×10^{-7}	0.23/1000 nm	1.18×10^{12}	[17]
PTB7-Th/L2	1.03	−1	1.2×10^{-13} [a]	0.09/980 nm	1.50×10^{11}	[24]
PTB7-Th/ATT-X-F_{in}	1.01	0	6.19×10^{-15} [a]	0.53/1110 nm	1.71×10^{13} [b]	[25]
PDPPDTP/TPCTO-2F	1.00	0	9.1×10^{-14} [a]	0.106/1060 nm	2.3×10^{11}	[26]
PCE10/BDP4Cl	1.00	0	3.58×10^{-10}	0.17/1100 nm	3.81×10^{12}	[27]
PBDT-TT:TBzIC	0.97	0	2.40×10^{-10}	0.23/1100 nm	2.55×10^{13}	[28]
PTB7-Th/TTD(DTC-2FIC)$_2$	0.95	−0.5	2.02×10^{-7}	0.0095/1100 nm	1.1×10^{11}	[29]
PCE10/COTIC-4Cl/PC$_{71}$BM	0.95	−0.1	1.1×10^{-8}	0.35/1050 nm	5×10^{12}	[30]
PTB7-Th/Y-QC4F	0.83	0	1.47×10^{-14} [a]	0.12/1200 nm	1.68×10^{12} /1160 nm	[31]

[a] Noise current. [b] Shot-noise-limited specific detectivity. [c] Measured at −2 V bias

15. ^{1}H NMR , ^{13}C NMR and mass spectra.

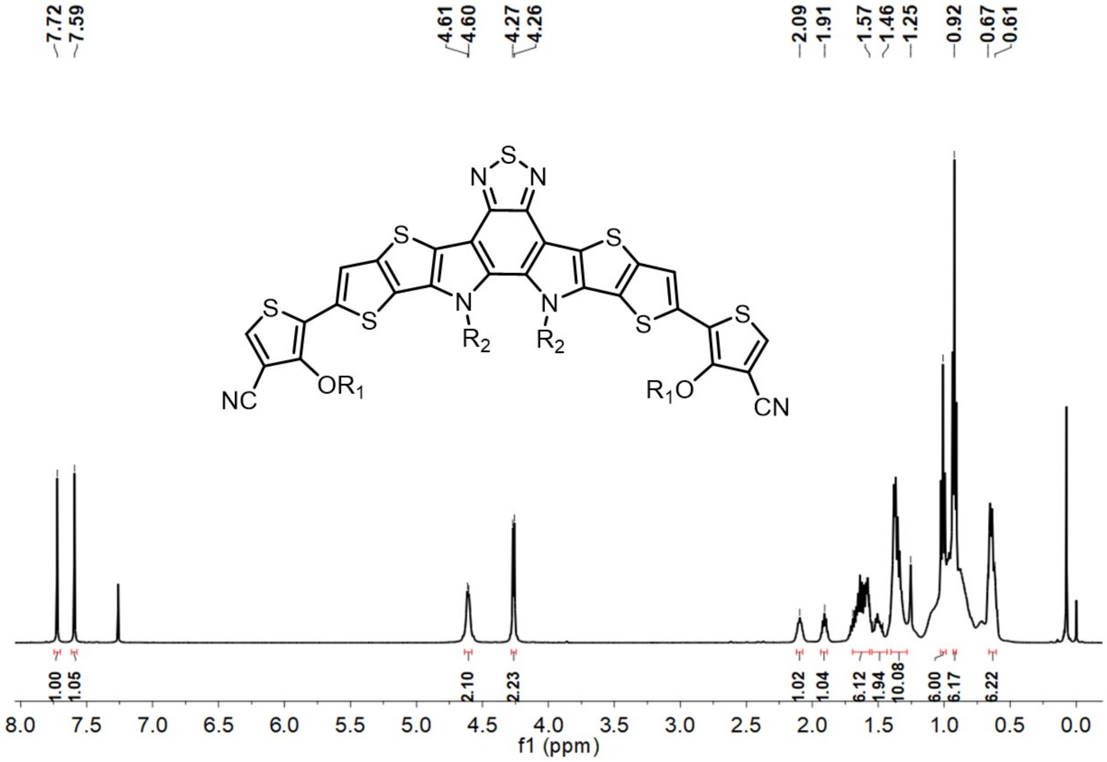

Figure S10. ^{1}H NMR of **3**.

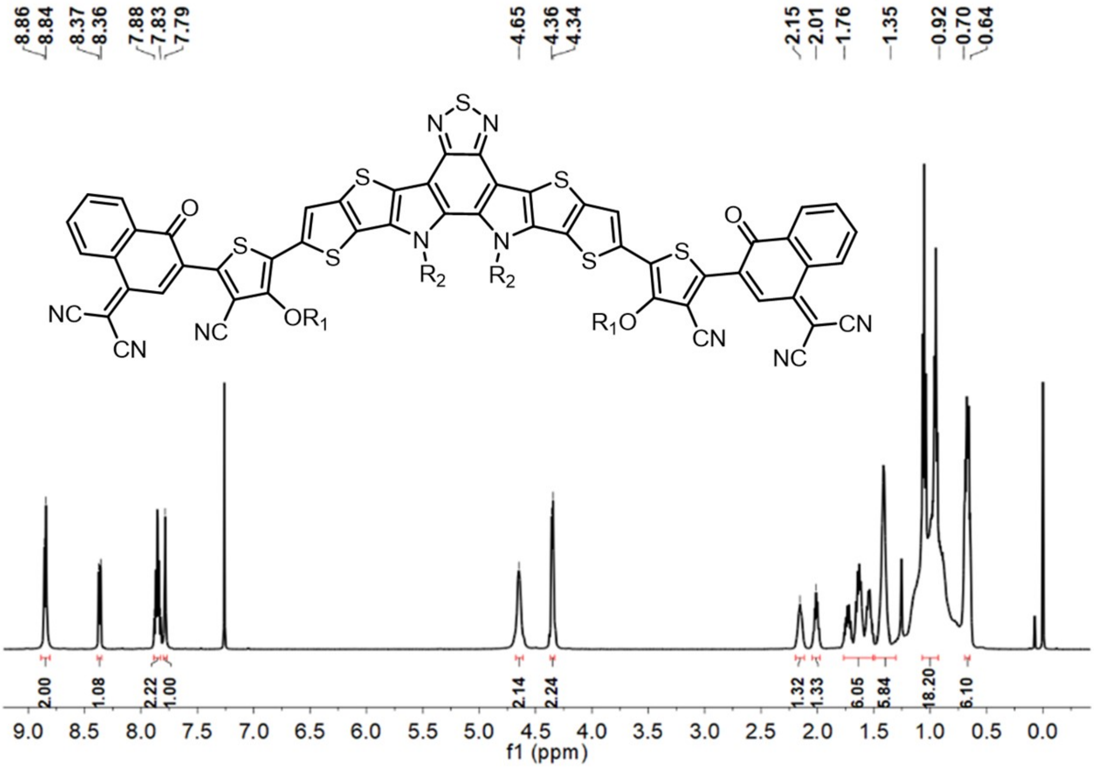
8.86
8.84
8.37
8.36
7.88
7.83
7.79
4.65
4.36
4.34
2.15
2.01
1.76
1.35
0.92
0.70
0.64
S
N
N
S
S
S
S
N
N
R_2
R_2
O
O
S
S
NC
CN
NC
OR_1
R_1O
CN
CN
NC
2.00
1.08
2.22
1.00
2.14
2.24
1.32
1.33
6.05
5.84
18.20
6.10
9.0 8.5 8.0 7.5 7.0 6.5 6.0 5.5 5.0 4.5 4.0 3.5 3.0 2.5 2.0 1.5 1.0 0.5 0.0
f1 (ppm)

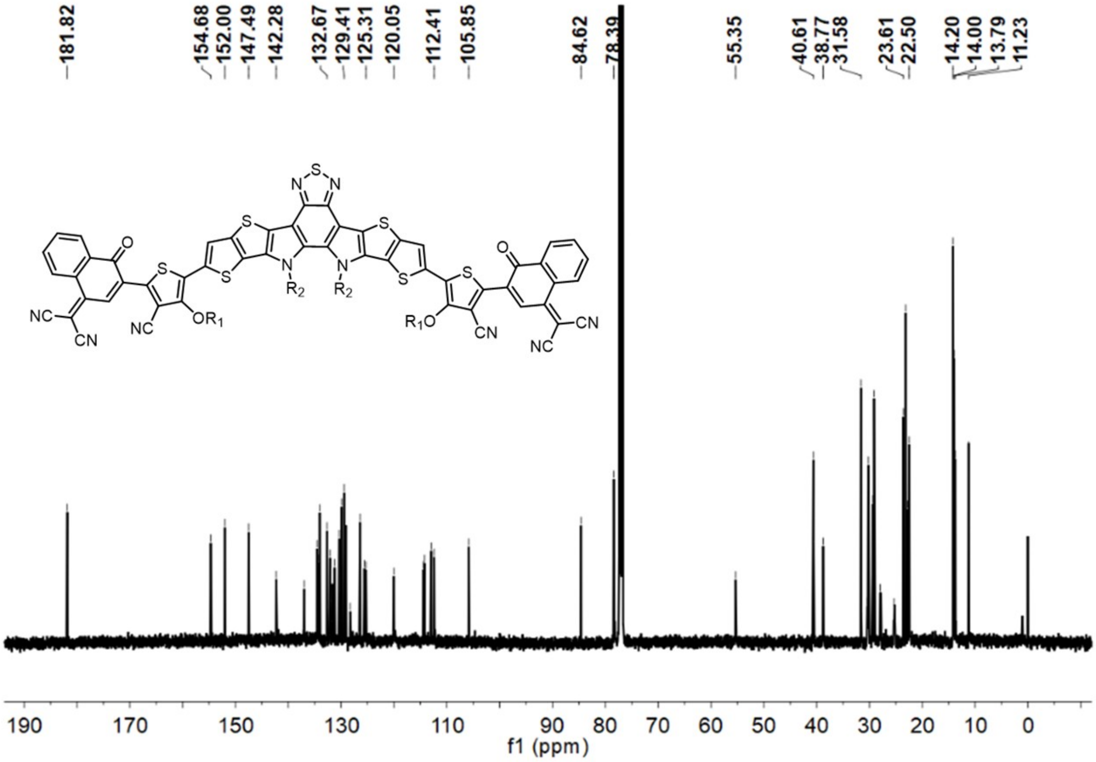
181.82
154.68
152.00
147.49
142.28
132.67
129.41
125.31
120.05
112.41
105.85
84.62
78.39
55.35
40.61
38.77
31.58
23.61
22.50
14.20
14.00
13.79
11.23
S
N
N
N
N
R_2
R_2
O
O
S
S
S
S
S
S
NC
CN
NC
OR_1
R_1O
CN
CN
NC
190 170 150 130 110 90 80 70 60 50 40 30 20 10 0
f1 (ppm)

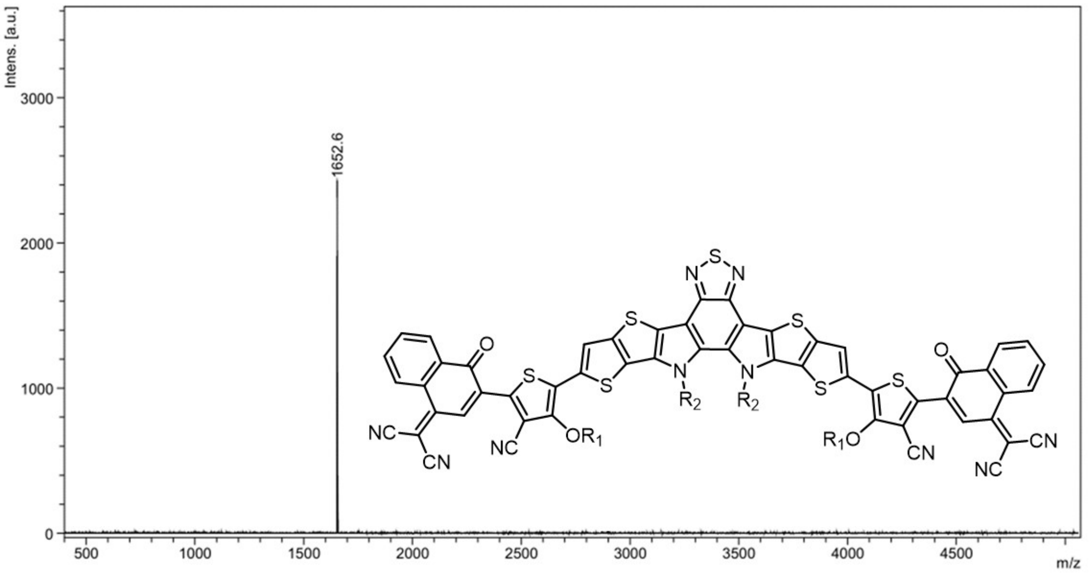

Figure S11. ^{1}H NMR , ^{13}C NMR and mass spectra of **BTQ-1**.

References

[1] Y. Xu, T. Zhang, H. Yao, J. Wang, P. Bi and J. Hou, *J. Energy Chem.*, 2022, **72**, 388-394.

[2] X. Zhu, Y. Zhang, H. Li, Y. Zhang, J. Miao, J. Liu and L. Wang, *Sci. Bul.*, 2024, **69**, 2679-2682.

[3] J.-W. Ha, A. Y. Lee, H. J. Eun, J.-H. Kim, H. Ahn, S. Park, C. Lee, D. W. Seo, J. Heo, S. C. Yoon, S.-J. Ko and J. H. Kim, *ACS Nano*, 2023, **17**, 18792-18804.

[4] Y. Zhang, Y. Yu, X. Liu, J. Miao, Y. Han, J. Liu and L. Wang, *Adv. Mater.*, 2023, **35**, 2211714.

[5] Y. Zheng, Y. Chen, Y. Cao, F. Huang, Y. Guo and X. Zhu, *ACS Mater. Lett.*, 2022, **4**, 882-890.

[6] S. Zhong, H. Chen, J. Yi, T. Yang, Z. Gan, X. Su, M. Li, Z. Zhong, F. Peng and L. Ying, *Org. Electron.*, 2022, **109**, 106610.

[7] Y. Chen, Y. Zheng, Y. Jiang, H. Fan and X. Zhu, *J. Am. Chem. Soc.*, 2021, **143**, 4281-4289.

[8] M. Babics, H. Bristow, W. Zhang, A. Wadsworth, M. Neophytou, N. Gasparini and I. McCulloch, *J. Mater. Chem. C*, 2021, **9**, 2375-2380.

[9] J. Lee, S.-J. Ko, H. Lee, J. Huang, Z. Zhu, M. Seifrid, J. Vollbrecht, V. V. Brus, A. Karki, H. Wang, K. Cho, T.-Q. Nguyen and G. C. Bazan, *ACS Energy Lett.*,

2019, **4**, 1401-1409.

[10] W. Wang, X. Miao, G. Cai, L. Ding, Y. Li, T. Li, Y. Zhu, L. Tao, Y. Jia, Y. Liang, X. Lu, Y. Fang, Y. Yi and Y. Lin, *Adv. Mater.*, 2022, **34**, 2201600.

[11] J. Huang, J. Lee, J. Vollbrecht, V. V. Brus, A. L. Dixon, D. X. Cao, Z. Zhu, Z. Du, H. Wang, K. Cho, G. C. Bazan and T.-Q. Nguyen, *Adv. Mater.*, 2020, **32**, 1906027.

[12] Y. Zhang, Q. Wei, Z. He, Y. Wang, T. Shan, Y. Fu, X. Guo and H. Zhong, *ACS Appl. Mater. Interfaces*, 2022, **14**, 31066-31074.

[13] Y. Xia, C. Geng, X. Bi, M. Li, Y. Zhu, Z. Yao, X. Wan, G. Li and Y. Chen, *Adv. Opt. Mater.*, 2024, **12**, 2301518.

[14] T. Liu, Z. Jia, Y. Song, N. Yu, Q. Lin, C. Li, Y. Jia, H. Chen, S. Wang, Y. Wei, Y. Lin, F. Huang, Z. Tang, Y. Li, L. Meng and H. Huang, *Adv. Funct. Mater.*, 2023, **33**, 2301167.

[15] L. Shao, L. Hong, Y. Cao, H. Tang, Y. Huang, X. Xia, Y. Bai, M. Dong, X. Zhang, X. Lu, X. Yang, C. Liu, F. Huang and Y. Cao, *Adv. Opt. Mater.*, 2023, **11**, 2202823.

[16] U.-H. Lee, B. Park, S. Rhee, J.-W. Ha, D. R. Whang, H. J. Eun, J. H. Kim, Y. Shim, J. Heo, C. Lee, B. J. Kim, S. C. Yoon, J. Lee and S.-J. Ko, *Adv. Opt. Mater.*, 2023, **11**, 2300312.

[17] J.-W. Ha, H. J. Eun, B. Park, H. Ahn, D. R. Hwang, Y. S. Shim, J. Heo, C. Lee, S. C. Yoon, J. H. Kim and S.-J. Ko, *Adv. Funct. Mater.*, 2023, **33**, 2211486.

[18] K. Cho, J.-W. Ha, M. Nam, C. Lee, S. J. You, A. Y. Lee, S. C. Yoon, M. Han, J. H. Kim, S.-J. Ko and D.-H. Ko, *Adv. Funct. Mater.*, 2024, **34**, 2400676.

[19] S. Deng, L. Zhang, J. Zheng, J. Li, S. Lei, Z. Wu, D. Yang, D. Ma and J. Chen, *Adv. Opt. Mater.*, 2022, **10**, 2200371.

[20] Y. Wang, M. Yang, B. Yin, B. Wu, G. Liu, S. Jeong, Y. Zhang, C. Yang, Z. He, F. Huang, Y. Cao and C. Duan, *ACS Appl. Mater. Interfaces*, 2024, **16**, 66846-66856.

[21] J. Xu, Y. Zhang, J. Liu and L. Wang, *Angew. Chem. Int. Ed.*, 2023, **62**, e202310838.

[22] L. Shao, J. Yang, Y. Huang, Y. Cao, J. Jing, X. Qin, X. Yang, H. Tang, C. Liu, F. Huang and Y. Cao, *Chem. Mater.*, 2024, **36**, 5775-5787.

[23] Y. Wang, J. Wang, J. Miao, J. Liu and L. Wang, *CCS Chemistry*, 2024, **6**, 2794-2803.

[24] T. Li, G. Hu, L. Tao, J. Jiang, J. Xin, Y. Li, W. Ma, L. Shen, Y. Fang and Y. Lin, *Sci. Adv.*, 2023, **9**, eadf6152.

[25] Y. Chen, Y. Zheng, J. Wang, X. Zhao, G. Liu, Y. Lin, Y. Yang, L. Wang, Z. Tang, Y. Wang, Y. Fang, W. Zhang and X. Zhu, *Sci. Adv.*, *10*, eadm9631.

[26] H. Hou, W. Wang, T. Li, Z. Zhang, X. Miao, G. Cai, X. Lu, Y. Yi and Y. Lin, *Angew. Chem. Int. Ed.*, 2025, **n/a**, e202425420.

[27] M. Yang, B. Yin, G. Hu, Y. Cao, S. Lu, Y. Chen, Y. He, X. Yang, B. Huang, J. Li, B. Wu, S. Pang, L. Shen, Y. Liang, H. Wu, L. Lan, G. Yu, F. Huang, Y. Cao and C. Duan, *Chem*, 2024, **10**, 1425-1444.

[28] B. Yin, X. Zhou, Y. Li, G. Hu, W. Wei, M. Yang, S. Jeong, W. Deng, B. Wu, Y. Cao, B. Huang, L. Pan, X. Yang, Z. Fu, Y. Fang, L. Shen, C. Yang, H. Wu, L. Lan, F. Huang, Y. Cao and C. Duan, *Adv. Mater.*, 2024, **36**, 2310811.

[29] H. Zhang, R. Mao, L. Yuan, Y. Wang, W. Liu, J. Wang, H. Tai and Y. Jiang, *ACS Appl. Mater. Interfaces*, 2024, **16**, 9088-9097.

[30] Z. Zhong, F. Peng, L. Ying, G. Yu, F. Huang and Y. Cao, *Sci. China Mater.*, 2021, **64**, 2430-2438.

[31] Y. Zhang, J. Chen, J. Yang, M. Fu, Y. Cao, M. Dong, J. Yu, S. Dong, X. Yang, L. Shao, Z. Hu, H. Cai, C. Liu and F. Huang, *Adv. Mater.*, 2024, **36**, 2406950.